RESEARCH ARTICLE

Modulating spin relaxation at the ferromagnet/molecule interface via anchoring atom engineering

Xurong Shi [1,4], Shen Wang [2,3,*], Kai Li [5], Chengdong Mi [1,4], Jinrong Wang [1,4]

[1] Department of Physics and Electronic Information Engineering, Lyuliang University, Lishi 033001, China

[2] School of Physics and Electronics Engineering, Shanxi University, Taiyuan 030006, China

[3] State Key Laboratory of Quantum Optics and Quantum Optics Devices, Shanxi University, Taiyuan 030006, China

[4] Lvliang City Key Laboratory of Quantum Precision Measurement, Lyuliang University, Lishi 033001, China

[5] College of Physics, Changchun Normal University, Changchun 130032, China

Corresponding author. E-mail: *shenwang@sxu.edu.cn

Received October 24, 2025; accepted March 17, 2026

Supporting Information

1. All isolated molecular energy levels

Table S1. Calculation results of the isolated carboxylic acids, sulfonic acids and sulfuric acids.

Molecule		HOMO(eV)	LUMO(eV)	Length(Å)	Gap(eV)	Dipole moment(D)
C	C4	−7.95	−0.29	8.58	7.66	1.35
	C8	−7.92	−0.29	13.70	7.63	1.32
	C12	−7.91	−0.19	18.83	7.72	1.32
	C18	−7.90	−0.19	26.53	7.71	1.32
S	S4	−8.68	−0.50	10.19	8.18	4.20
	S8	−8.55	−0.49	15.26	8.06	4.38
	S12	−8.30	−0.48	20.34	7.82	4.44
	S16	−8.11	−0.48	25.41	7.63	4.46
SO	SO4	−8.68	−0.68	10.80	8.00	3.73
	SO8	−8.66	−0.68	15.84	7.98	3.87
	SO12	−8.31	−0.67	20.94	7.64	3.91
	SO16	−8.10	−0.67	26.03	7.43	3.92

The density functional theory (DFT) calculations for these complexes were performed using the Guassian16 package [1]. The geometry optimizations and frequency calculations were conducted using the B3LYP/6-311+G(d, p) basis sets [2, 3].

2. Carrier transport mechanisms: tunneling

1) Fig. 2(b) shows that the dependence of resistivity (ρ) on molecular length (d), followed $\rho \sim e^{-\beta d}$, and β is temperature-independent (Table S2), demonstrating that the carriers are tunneling through molecules from one Fe_3O_4 particle to another.

Table S2. Comparison of attenuation coefficients of different anchoring groups.

Temperature	295K	250K	200K	Average
β_C (Å^{-1})	0.195	0.210	0.215	0.21
β_S (Å^{-1})	0.267	0.263	0.254	0.26
β_{SL} (Å^{-1})	0.229	0.235	0.229	0.23

2) The temperature dependence of ρ is governed by the intrinsic properties of Fe_3O_4 rather than carrier transport within the molecules. Figure S1 shows ρ as a function of temperature (T) in the semi-log plots for S(C4), S(S4), and S(SO4). The almost linear relationships for all samples mean that ρ increases exponentially with decreasing T. And all the curves show almost the identical slope, including other samples not shown in Figure S1, independent on the types of the molecules, the nature of the particle-to-particle contacts and the size of Fe_3O_4 nanoparticles [4], which should be arisen from the common constituent material in all samples--Fe_3O_4. A similar exponentially increased ρ is also observed in La0.7Sr0.3MnO3/NiFe2O4/Fe_3O_4 magnetic tunnel junction devices [5]. So the exponentially increasing ρ should be explained by the decreasing density-of-states (DOS) of Fe_3O_4 at the Fermi level observed in photoemission spectroscopy or the ~ 0.2 eV band gap of Fe_3O_4 [6].

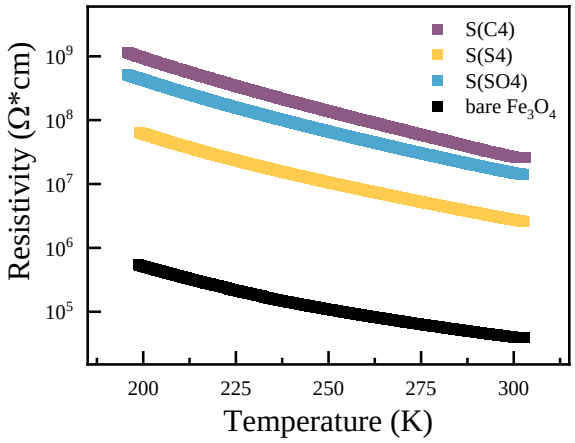

Figure S1. A plot of ρ as a function of T for S(C4), S(S4), and S(SO4).

3) The current-voltage (I-V) curves for S(C4), S(S4) and S(SO4) at 300K are displayed in Figure S2, the nearly linear I-V curves are consistent with tunneling behavior at low bias. Although a voltage of 200 V was applied across the sample, the voltage across each Fe_3O_4/molecules/Fe_3O_4 junction is estimated to be only a few millivolts, considering the sample dimensions ($7 \times 7 \times 1$ mm^3), molecular length, and Fe_3O_4 nanoparticle diameter (10 nm).

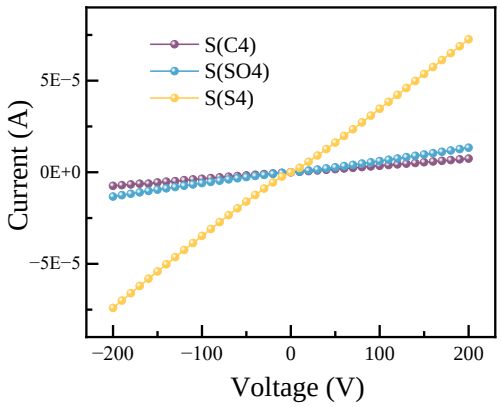

Figure S2. the *I-V* curves for S(C4), S(S4) and S(SO4) at 300K.

Consequently, we conclude that the carriers tunneling through the organic molecules, rather than hopping.

Furthermore, it should be the intramolecular tunneling, rather than the intermolecular tunneling transport for several reasons. Firstly, since the molecules are chemically-bonded to Fe_3O_4 nanoparticles, the dominant transport mechanism is the "through-bond" tunneling. Secondly, the *d*-dependent resistivity and the different β values further exclude intermolecular tunneling [7]. Finally, the *MR* of Fe_3O_4 coated with molecules is significantly larger than the bare Fe_3O_4 (~4% at 300K) [8], if intermolecular tunneling were dominant, the *MR* would be comparable to that of the bare Fe_3O_4 particles.

3. Computational details and model

Computational Details

The calculations were carried out using density functional theory with the PBE+U form of generalized gradient approximation functional (GGA) [9]. The Vienna ab-initio simulation package (VASP) [10-13] was employed. The effective U value is calculated by the linear response approach and the U value is 4.74 eV for Fe-3d orbital [14]. The plane wave energy cutoff was set as 400 eV. The Fermi scheme was employed for electron occupancy with an energy smearing of 0.1 eV. The first Brillouin zone was sampled in the Monkhorst−Pack grid [15]. The 3×3×1 k-point mesh for the surface calculation. The energy (converged to 1.0 $\times 10^{-6}$ eV/atom) and force (converged to 0.01eV/Å) were set as the convergence criterion for geometry optimization. The spin polarization was considered in all calculation. The Crystal Orbital Hamilton Population (COHP) [16, 17] is calculated based on the program of LOBSTER [18]. For COHP, the negative (positive) value means the bonding (anti-bonding) state. The bond strength can be estimated by the integrated COHP (ICOHP), i.e., the more negative of ICOHP, the stronger of the bond.

Model

The Fe_3O_4(111) is selected as the adsorption surface, whose model is obtained by cutting Fe_3O_4 bulk along the [111] direction [19-21]. In surface model, the three layers will be employed with the bottom layer fixed. For molecule adsorption, the Fe atom in the surface was selected as the active site.

4. Charge transfer at the Fe_3O_4/molecule interface

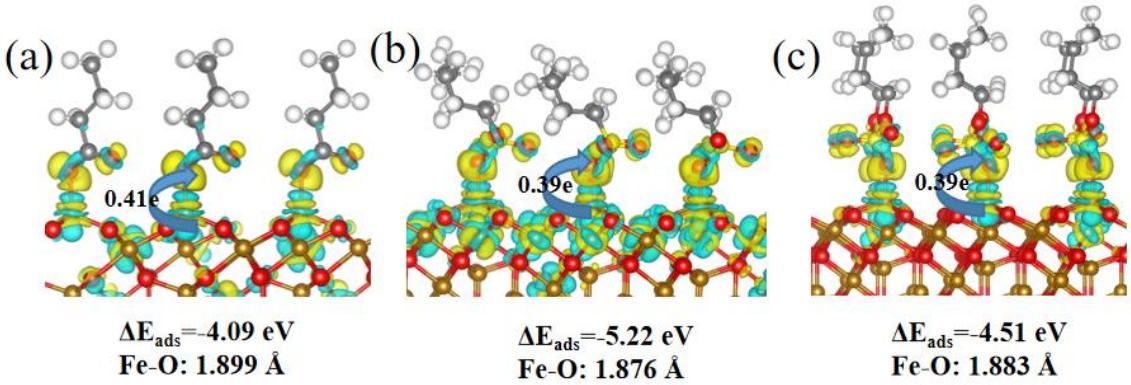

Figure S3. The differential charge of Fe_3O_4—COOH, Fe_3O_4—SO_3H and Fe_3O_4—OSO_3H, respectively. The yellow and blue area denotes the electronic accumulation and deficiency, respectively.

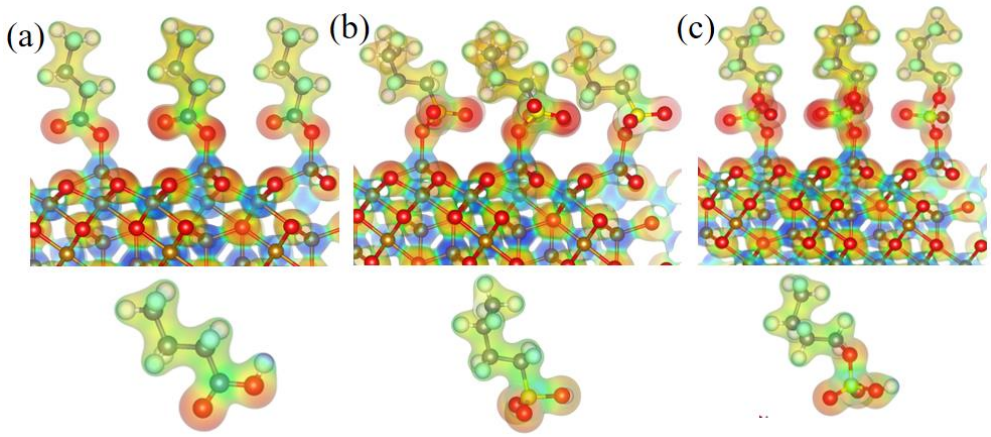

Figure S4. The electrostatic potential of Fe_3O_4—COOH, Fe_3O_4—SO_3H and Fe_3O_4—OSO_3H, and the corresponding isolated molecule.

The chemical adsorption will induce charge transfer at the Fe_3O_4/molecule interface (Figure S3), where electrons are transferred from Fe_3O_4 to the adsorbed molecules. The resulting electrostatic potential at Fe_3O_4/molecule interface is shown in Figure S4.

5. Effect of surface modification on magnetic properties

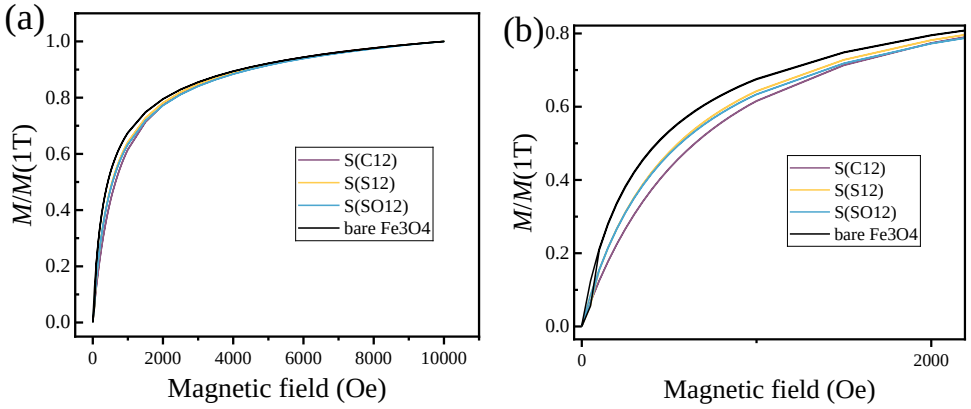

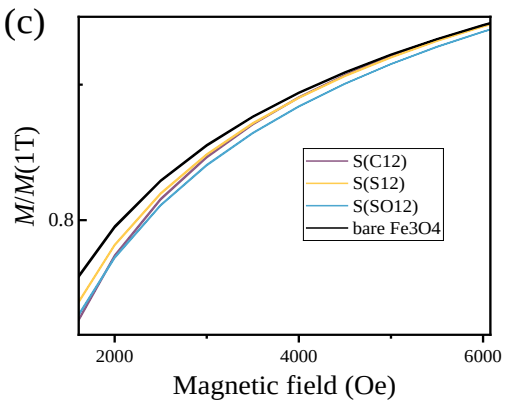

Figure S5. (a) Normalized magnetization curves of these samples, magnified views in the 0-2000 Oe (b) and 2000-6000 Oe (c) ranges.

Figure S5 shows the normalized magnetization curves for bare Fe_3O_4, S(C12), S(S12) and S(SO12). In the low-field range of 0-2000 Oe, bare Fe_3O_4 exhibits the fastest magnetization response, followed by S(S12) and S(SO12), while S(C12) shows the slowest increase. Correlating these results with the mass loss ratios obtained from TGA, it can be inferred that the coated density of S(C12) is approximately twice that of S(S12) and S(SO12). This indicates that carboxylic acid forms a higher density of Fe-O chemical bonds on the Fe_3O_4 particle surfaces, leading to a significantly larger proportion of surface magnetic moments. Consequently, we speculate that the low relative magnetization of S(C12) in this range is mainly due to the surface magnetic moment effect.

As the magnetic field further increases (2000-6000 Oe), the relative magnetization growth rate of S(C12) exceeds those of S(SO12) and S(S12). This suggests that despite the surface magnetic moment proportion is the highest, the magnetic moments in S(C12) are more susceptible to field-induced alignment compared to the latter two samples—a trend corroborated by the observed M_{S1}(C12) > M_{S1}(S12) > M_{S1}(SO12). We speculate that this behavior is closely related to the interfacial Fe-O bonding strength: stronger bonding might induce a more pronounced pinning effect on surface magnetic moments, thereby suppressing the saturation magnetization (M_{S1}). In contrast, S(SO12) exhibits the lowest relative magnetization in this range, indicating that its surface magnetic moment is the most difficult to align with magnetization, and M_{S1} is also the lowest. However, although the bonding strength of S(S12) is stronger than that of S(SO12), its saturation magnetization is greater, which implies the presence of other underlying factors that need to further investigation.

6. The rationality for extending the carboxylic acid series to C18

Regarding the extension of the carboxylic acid series to C18 rather than C16, the reasons are as follows:

1) The S(C16) had a low success proportion in preparation and subsequent magneto-transport measurements (only two sets), resulting in insufficient valid data sets for meaningful statistical analysis. Therefore, it was not included in our research. In contrast, we obtained dozens of reliable magneto-transport datasets for S(C18), which offer significantly higher data quality and statistical reliability.

2) We have extracted the spin diffusion length (λ) by fitting the magnetoresistance data of S(C4), S(C8), S(C12), and S(C18), as shown in Figure S6. It is evident that there is indeed a difference of approximately 4.1 nm in the average λ values obtained using S(C16) and S(C18) respectively, with the data dispersion (standard deviation) being greater for the C16 combination. We believe that this discrepancy primarily resulted from the scarcity of high-quality and reproducible data available for S(C16), which introduces significant uncertainty, rather than the physical intrinsic changes caused by the increase in chain length from C16 to C18.

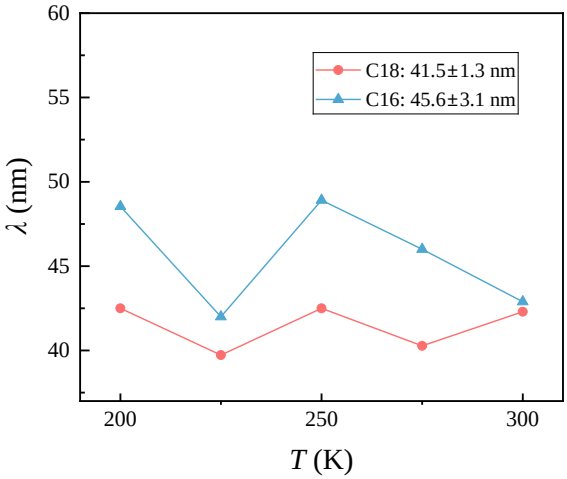

Figure S6. Comparison of λ-T curves: red, extended to C18; blue, extended to C16.

References

[1] M. J. Frisch, G. W. Trucks, H. B. Schlegel, et al. Gaussian 16 (2016).

[2] A. D. Becke. Density-functional thermochemistry. I. The effect of the exchange-only gradient correction, J. Chem. Phys. 96(3), 2155 (1992).

[3] R. Krishnan, J. S. Binkley, R. Seeger, J. A. Pople, Self-consistent molecular orbital methods. XX. A basis set for correlated wave functions, J. Chem. Phys. 72(1), 650 (1980).

[4] F. J. Yue, S. Wang, D. Wu, Spin transport in molecules studied by Fe3O4/molecule nanoparticles, Appl. Phys. A, 111(2), 347 (2013).

[5] B. B. Nelson-Cheeseman, F. J. Wong, R. V. Chopdekar, E. Arenholz, Y. Suzuki, Room temperature magnetic barrier layers in magnetic tunnel junctions, Phys. Rev. B, 81, 849 (2010).

[6] A. Chainani, T. Yokoya, T. Morimoto, T. Takahashi, S. Todo, Electronic structure of Fe3O4 across the verwey transition, J Electron Spectrosc Relat Phenom, 78, 99 – 102 (1996).

[7] X. Shi, F. Chen, S. Wang, Y. Shi, X. Su, H. Zhou, H. Jiao, Enhancement of spin diffusion length in tunneling junctions by benzene ring insertion into the saturated alkyl sulfonic acid, Appl. Phys. Express, 15(7), 073001 (2022).

[8] X. Shi, S. Wang, X. Su, Y. Shi, B. Shi, H. Zhou, and H. Jiao, Interfacial oxidation for spin transport in Fe3O4/sulfonic acid molecule nanoparticles, Solid State Electronics 177, 107962 (2021).

[9] J. P. Perdew, K. Burke, Ernzerhof M. Generalized Gradient Approximation Made Simple, Phys. Rev. Lett. 77, 3865 (1996).

[10] G. Kresse, J. Furthmüller, Efficiency of Ab-initio Total Energy Calculations for Metals and Semiconductors Using a Plane-Wave Basis Set, *Comp. Mater. Sci.* 6, 15 (**1996**).

[11] G. Kresse, J. Hafner, Ab initio Molecular Dynamics for Liquid Metals, Phys. Rev. B 47, 558 (1993).

[12] G. Kresse, J. Hafner, Ab initio Molecular-Dynamics Simulation of the Liquid-Metal–Amorphous-Semiconductor Transition in Germanium, Phys. Rev. B, 49, 14251 (1994).

[13] G. Kresse, J. Furthmüller, Efficient Iterative Schemes for Ab Initio Total-Energy Calculations Using a Plane-Wave Basis Set, Phys. Rev. B, 54, 11169 (1996).

[14] M. Cococcioni, S. de Gironcoli, Linear response approach to the calculation of the effective interaction parameters in the LDA+U method, Phys. Rev. B, 71, 035105 (2005).

[15] H. J. Monkhorst, J. D. Pack, Special Points for Brillouin-Zone Integrations, Phys. Rev. B, 13, 5188 (1976).

[16] R. Dronskowski, P. E. Blöchl, Crystal orbital hamilton populations (COHP): Energy-resolved visualization of chemical bonding in solids based on density-functional calculations, J. Phys. Chem. 97,

8617 (1993).
[17] V. L. Deringer, A. L. Tchougreeff, R. Dronskowski, Crystal orbital hamilton population (COHP) analysis as projected from plane-wave basis sets, J. Phys. Chem. A 115, 5461 (2011).
[18] S. Maintz, V. L. Deringer, A. L. Tchougreeff, R. Dronskowski, LOBSTER: A tool to extract chemical bonding from plane-wave based DFT, J. Comput. Chem. 37, 1030 (2016).
[19] D. Santos-Carballal, A. Roldan, R. Grau-Crespo, N. H. De Leeuw, A DFT study of the structures, stabilities and redox behaviour of the major surfaces of magnetite Fe3O4, Physical Chemistry Chemical Physics, 16(39), 21082 (2014).
[20] Z. H. Dastgerdi, S. S. Meshkat, S. Hosseinzadeh, M. D. Esrafili, Application of novel Fe3O4–polyaniline nanocomposites in asphaltene adsorptive removal: equilibrium, kinetic study and DFT calculations, Journal of Inorganic and Organometallic Polymers and Materials, 29(4), 1160 (2019).
[21] M. Sun, X. Wang, W. Mi, Large magnetoresistance in Fe3O4/4, 4′-bipyridine/Fe3O4 organic magnetic tunnel junctions, The Journal of Physical Chemistry C, 122(5), 3115 (2018).